Supplementary Information

Experimental Section

Materials

Sulfuric acid (H_2SO_4, 98%), potassium sulfate (K_2SO_4, 99%), magnesium carbonate hydroxide ($Mg_2(OH)_2CO_3$, >99%), triethylamine ($C_6H_{15}N$, 99%), isopropanol (C_3H_8O, ≥99.7%), N, N-dimethylformamide (DMF, 99%) and N, N-dimethylacetamide (DMAc) were purchased from Sinopharm Chemical Reagent Co., Ltd. Nafion solution (5 wt%) and PVDF were purchased from Sigma-Aldrich. Oxalic acid ($H_2C_2O_4$, 98%) was purchased from Macklin. Gas diffusion electrode (YLS-30T) and cation-exchange membrane (Nafion HP) were purchased from Suzhou Sinero, Co., Ltd. High-purity CO_2 (99.99%), N_2 (99.999%) and Ar (99.999%) were provided by Linde gas Co., Ltd. All chemicals and materials were used as received without further purification. Ultrapure water (18.2 MΩ) was obtained using a Sartorius ultrapure water system.

Synthesis of the Ni-N-C nanocages

N-doped carbon nanocages (NC) were synthesized via chemical vapor deposition under argon atmosphere (100 mL/min) using magnesium carbonate hydroxide (1 g) and triethylamine (6 mL) as the template and carbon source, respectively. Triethylamine was injected into the tube furnace when the temperature reached 500 °C. The furnace was further heated to 1000 °C with a ramping rate of 10 °C/min, and kept at 1000 °C for 2 hours to obtain MgO@NC. NC was collected by washing with 2 M HCl to remove MgO. NiPc was loaded onto the NC nanocages through π-π interaction by mixing the dispersion of NiPc/DMF (8 mg/mL) and NC/DMF (3 mg/mL) and stirring for 24 hours at room temperature. The resulted NiPc/NC was collected by filtration and washed with DMF and ethanol, respectively. Afterwards, the NiPc/NC composite was calcined under argon atmosphere at 900 °C for 2 hours to obtain the Ni-N-C nanocages.

Fabrication of the IrO_2/Ti electrode

Titanium felt (3 cm × 3 cm) was cleaned in the boiled oxalic acid solution (0.5 mol/L) for 1 h. Then, $IrCl_3$ (30 mg) was dissolved in isopropanol (10 mL) containing 10% concentrated HCl (volume fraction). After that, the cleaned Titanium felt was soaked in the above $IrCl_3$ solution for 5 min, dried at 100 ℃ for 10 min and calcined in air at 500 ℃ for 2 h. This process was repeated until the loading of IrO_2 on the titanium felt reached 1 mg cm^{-2}.

Synthesis of anion exchange nanofibers (AENFs)

MTCP-50[1] (1 g) and PVDF (1 g) were dispersed in DMF (9 g) and DMAc (9 g) via ball milling for 3 h. The dispersion was then electrospun into nanofiber membrane (AENFs) at 15.3 kV with an injecting rate of 0.01 mL/min. AENFs was dried at 60 °C in vacuum oven overnight. AENFs with different thickness were prepared by varying the amount of spinning solution. AENFs with different MTCP-50/PVDF ratios

were prepared by tuning the ratio of MTCP-50/PVDF in the electrospinning precursor. Before use, AENFs were activated in 1 M KOH for more than 12 hours, and then washed thoroughly with ultrapure water to remove the excessive KOH.

Material characterization

The morphological characterizations were carried out by using scanning electron microanalyzer (SEM, FEI) at an accelerating voltage of 10 kV. Transmission electron microscope (TEM) and HAADF-STEM images were collected by using FEI Titan Themis Cubed G2 300 operated at 300 kV. The crystal structure was analyzed by powder XRD measurements with a Bruker D8 Advance X-ray diffractometer using Cu-Ka radiation and performed at a scanning rate of 0.02 °/s. XPS was carried out on an Escalab 250Xi X-ray photoelectron spectrometer (Thermo Fisher) with Al Ka (1486.6 eV) X-rays as the excitation source. The amount of K^+ was quantified by ICP-OES with an OPTIMA 8000 analyzer (PerkinElmer Inc.). X-ray absorption spectroscopy (XAS) was collected at Beamline 11B in Shanghai Synchrotron Radiation Facility (SSRF).

Electrochemical characterization

All electrochemical tests were conducted using the DH7001A electrochemical workstation. OH^- conductivity is measured by the AC impedance method using the electrochemical workstation[1]. Catalyst inks were prepared by dispersing 4 mg of the catalyst in a solution containing 1 mL isopropanol and 60 μL of 5 wt% Nafion under ultrasonication for 30 min. The catalyst ink was then drop-casted on the gas diffusion electrode and dried at 80 °C. High-purity CO_2 (60 mL min^{-1} for 5-cm^2 MEA and 100 mL min^{-1} for 25-cm^2 MEA) was supplied to the cathode gas flow channel. The electrolyte of K_2SO_4/H_2SO_4 K_2SO_4/H_2SO_4 ($C_{K^+} = 0.05\ M$, pH = 2) with a flow rate of 12 mL/min is pumped through a dual channel peristaltic pump into the anolyte flow channel. For MEA tests, the Ni-N-C cathode and IrO_2/Ti anode were separated by the cation exchange membrane (Nafion-HP) or the as-fabricated bipolar membranes. Anion exchange nanofibers of various thickness and composition were studied. The cell voltages of MEA are reported without iR correction. Gas products were quantified by using gas chromatography equipped with both flame ionization and thermal conductivity detectors (Agilent 7890B).

Evaluating H^+ migration through the AENFs

The H^+ migration rates across the anion-exchange nanofibers (AENFs) membranes were evaluated using a membrane-electrode assembly (MEA) configuration[2]. Each AENFs membrane was paired with a Nafion HP membrane, with 0.75 M H_2SO_4 circulated on the Nafion HP side and deionized (DI) water (18.2 MΩ·cm resistivity) on the AENFs side at a flow rate of 5 mL/min. The pH of the DI water compartment was monitored in real-time using a calibrated pH electrode (±0.01 accuracy) at 5-minute intervals over 30 minutes under thermostatic conditions (25±0.5°C).

Estimation of K^+ crossover and water flooding in MEA

A graduated liquid trap was integrated at the cathode exhaust port of the MEA to monitor phase-segregated fluids. During each galvanostatic eCO_2R test, cathodic effusion was collected from the reservoir at 5-hour intervals over a 15-hour operational period, yielding three sequential measurements per sample. The accumulated liquid volume was defined as the water flooding volume, while K^+ concentration in the collected liquid was determined via the inductively coupled plasma-atomic emission spectrometry (ICP-OES). Subsequently, the water flooding rate (mL/h) and K^+ crossover rate (mmol/h) were calculated by normalizing the total flooding volume and K^+ content against the total operation time. To ensure experimental robustness, triplicate measurements were conducted for each anion-exchange nanofibers (AENFs) variant under identical experimental configurations, with data presented as mean ± standard deviation across biological replicates.

Supplementary Note

The total cell voltage of MEA with AENF-1/CEM and CEM- only configuration was systematically deconvoluted according to the literature.[3] The total cell voltage of the MEAs is deconvoluted into to thermodynamic voltage, cathode overpotential, anode overpotential, ohmic loss, Nernstian pH loss, and other interfacial losses. The breakdown of cell voltages for different MEA configurations: CEM-only (3.23 V) and AENFs/CEM (3.51 V) at 100 mA/cm^2 are summarized in **Figures S19** and **Figure S20**.

Thermodynamic voltage: The thermodynamic voltage for eCO_2R to CO (-0.11 V vs RHE) and OER (1.23 V vs RHE) is 1.34 V.

Cathode Overpotential (η_c): The η_c was measured in a three-compartment flow cell using 1 M $KHCO_3$, FAA-3-PK-130, and 1 M KOH as cathode electrolyte, AEM and anode electrolyte, respectively. Catalyst-covered GDE, Ag/AgCl with saturated KCl, nickel foam was used as cathode, reference electrode and anode, respectively. iR compensation was applied using high-frequency resistance (HFR) derived from electrochemical impedance spectroscopy (EIS). At 100 mA/cm^2, the cathode overpotential was determined to be 0.48 ± 0.10 V (**Figure S16**).

Anode Overpotential (η_a): The η_a was evaluated in a three-electrode system using IrO_2/Ti, graphitic rod, Ag/AgCl and 0.5 M H_2SO_4 as the working electrode, counter electrode, reference electrode and electrolyte, respectively. At 100 mA/cm^2, the anode overpotential was measured as 0.52 ± 0.06 V (**Figure S17**).

Ohmic Losses (η_{ohm}): The η_{ohm} including the resistance of the membrane and electrode/membrane interface for AENFs/CEM and CEM-only configuration was calculated by multiplying the HFR (Ω cm^2) measured under operando condition at 100 mA/cm^2 (**Figure S18**). The η_{ohm} for AENF-1/CEM and CEM-only configuration were 0.42 ± 0.01 V and 0.16 ± 0.02 V, respectively. The voltage loss of the AENF-1 was estimated to be ~0.26 V.

Nernstian pH Loss: Assuming the cathode pH was 12 according to the previous modelling results,[4] the Nernstian pH loss arising from the pH gradient between the cathode surface and bulk catholyte, was estimated to be 0.59 V using the following equation.[5]

$$V_{Nernstian} = 0.059 \times (pH_{surface} - pH_{bulk})$$

Under CEM-only configuration, the sum of the above voltages is 3.09 V which is 0.14 V lower than the experimentally measured voltage of 3.23 V. Under AENF-1 configuration, the sum of the above voltages is 3.35 V which is 0.16 V lower than the experimentally measured voltage of 3.51 V.

Supplementary figures

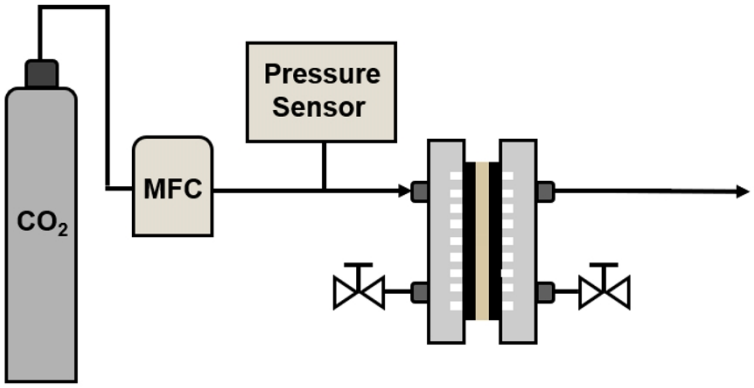

Figure S1. Schematic diagram illustrating the setup to assess the gas permeability of AENFs under their wetted states using a MEA fixture by recording the differential pressure between the

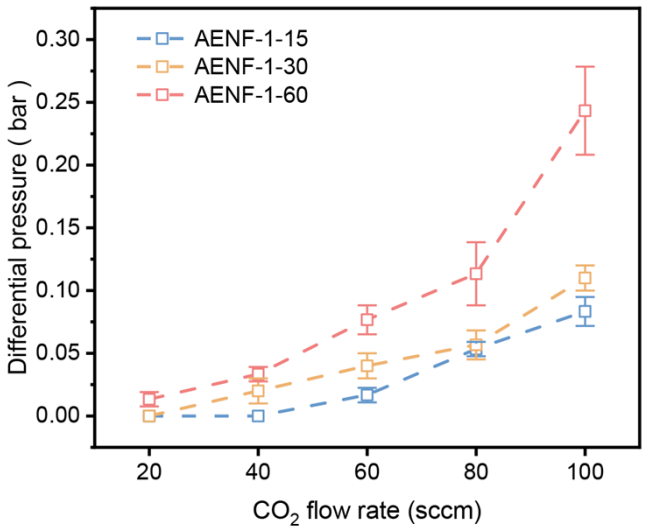

gas inlet and outlet of the MEA.[6]

Figure S2. Differential pressure measured for of AENF-1-*y* under different CO_2 flow rate.

Figure S3. Optical image showing the tensile test of AENF-1-*y* under their wetted states.

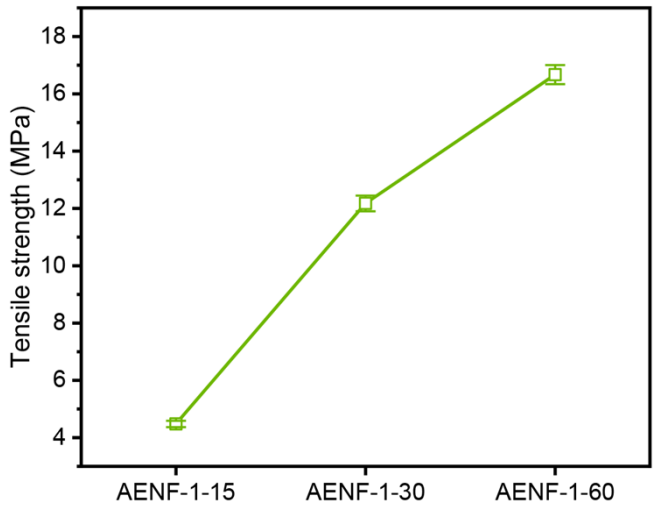

Figure S4. Tensile strengths of AENF-1-*y* with varying film thickness in the wet state.

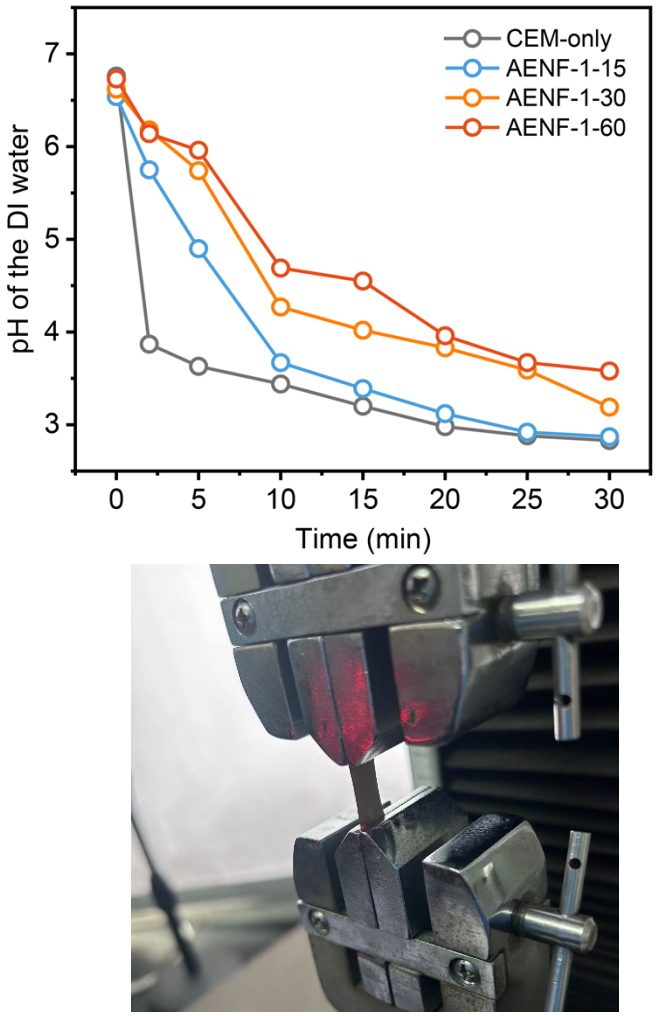

Figure S5. Bulk pH of the cathode electrolyte as a function of time for AENF-1-*y*.

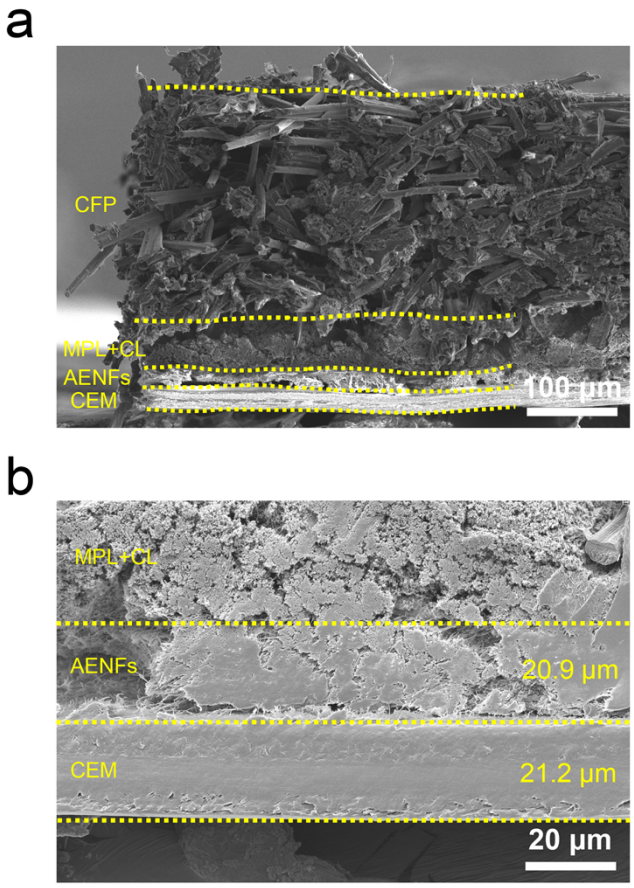

Figure S6. Cross-sectional SEM images of GDE/CL/AENF-1/CEM. (a) Panorama of carbon fiber paper (CFP), microporous layer (MPL), catalyst layer (CL) supported on microporous layer (MPL), AENFs layer, and CEM. (b) Enlarged SEM image of MPL, AENFs and CEM.

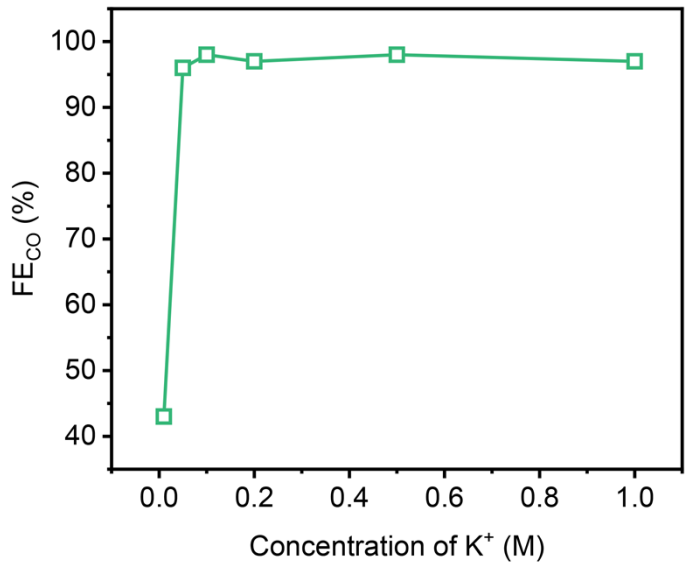

Figure S7. Faradaic efficiency of CO at different K^+ concentrations.

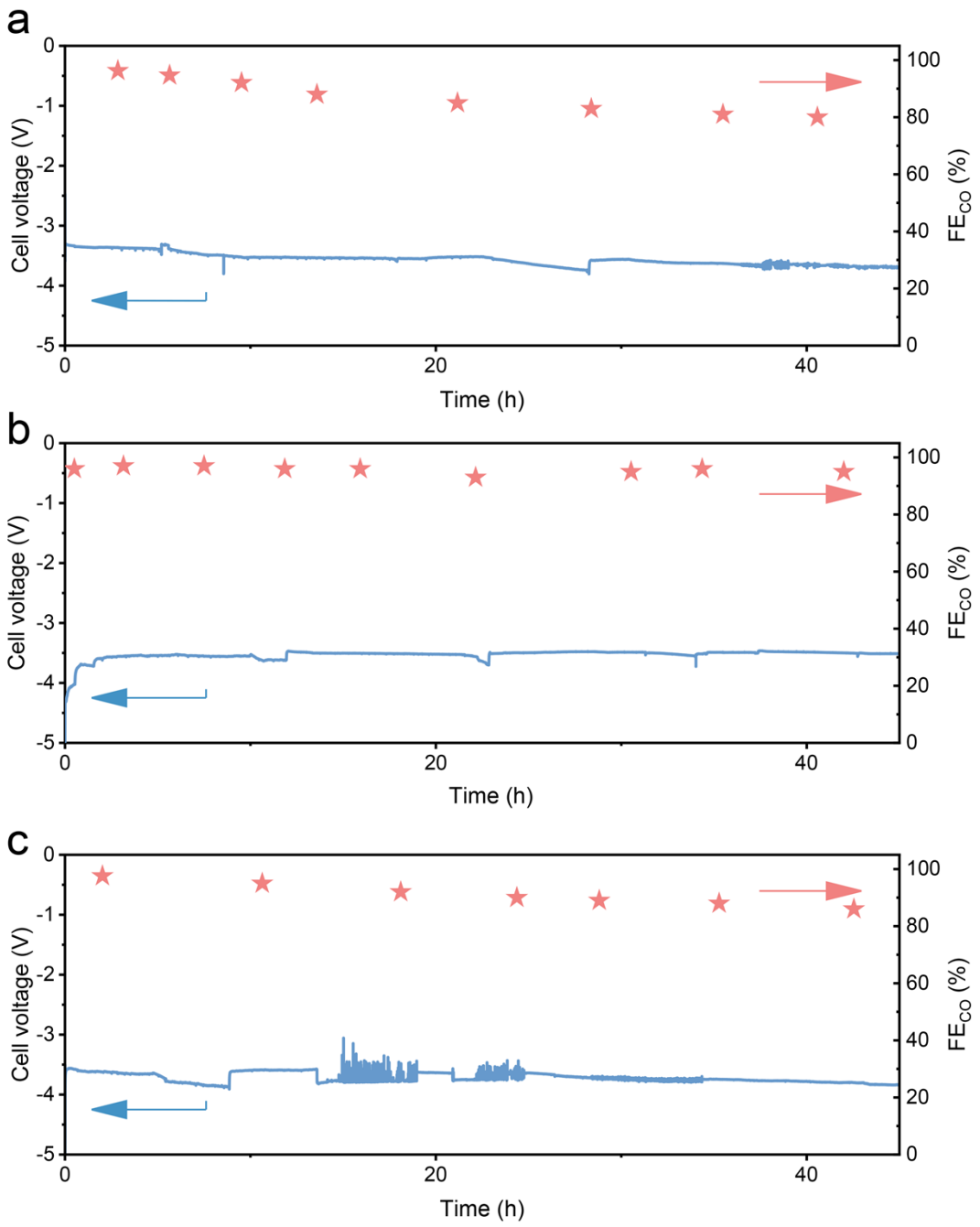

Figure S8. Galvanostatic eCO_2R tests of AENF-1-*y* in a 5-cm^2 acidic MEA at 100 mA/cm^2. (a) AENF-1-15, (b) AENF-1-30, (c) AENF-1-60.

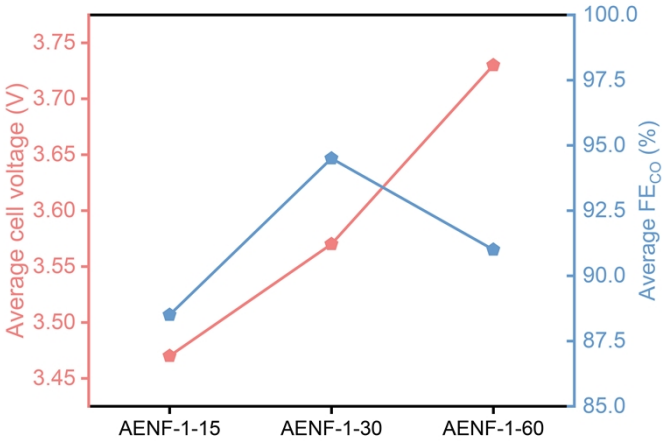

Figure S9. The average cell voltage and FE_{CO} of AENF-1-*y* measured during the 45-h galvanostatic eCO_2R test at 100 mA/cm^2.

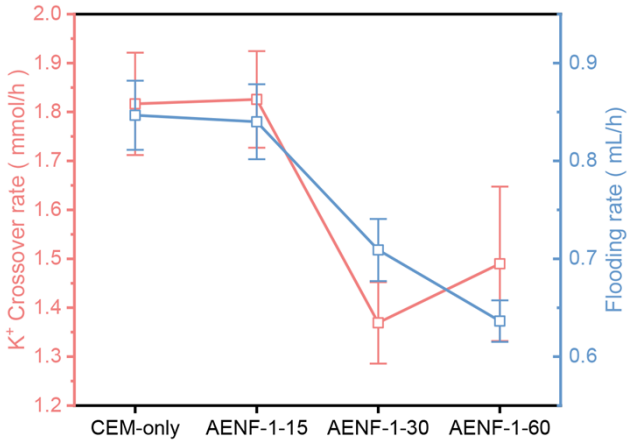

Figure S10. The K^+ crossover and flooding rates measured for AENF-1-*y* during the 45-h galvanostatic eCO_2R test at 100 mA/cm^2.

Figure S11. Top-view SEM images of AENF-*x*. (a) AENF-0.5, (b) AENF-1, (c) AENF-2 (d) AENF-3.

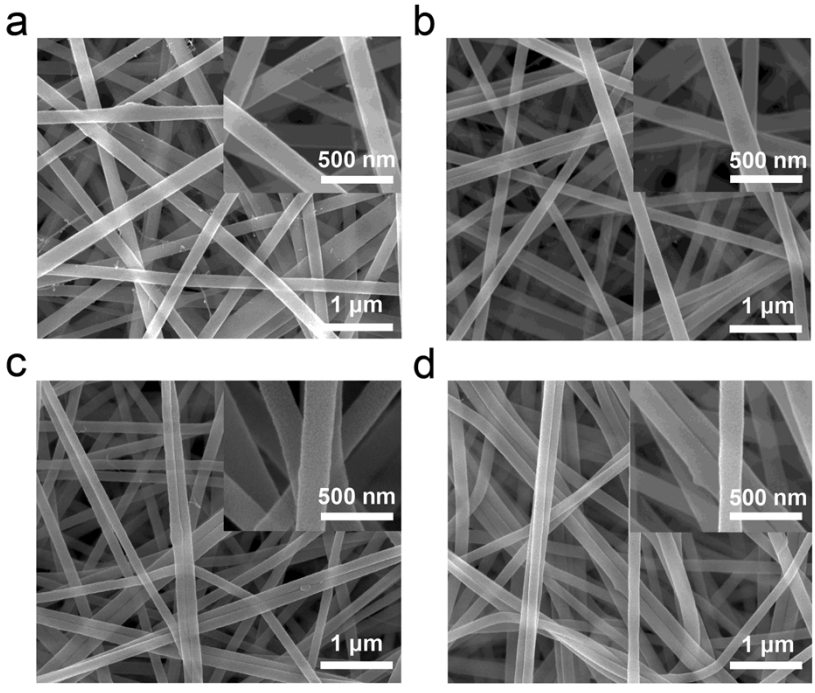

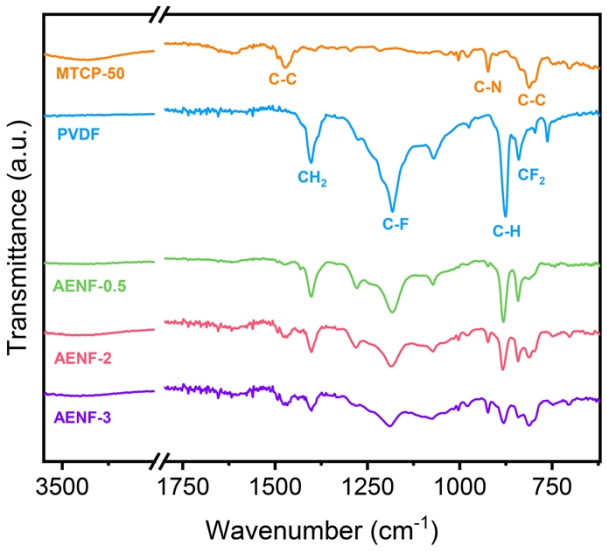

Figure S12. Infrared (IR) spectra of AENF-0.5, AENF-2 and AENF-3 in reference to MTCP-50 and PVDF.

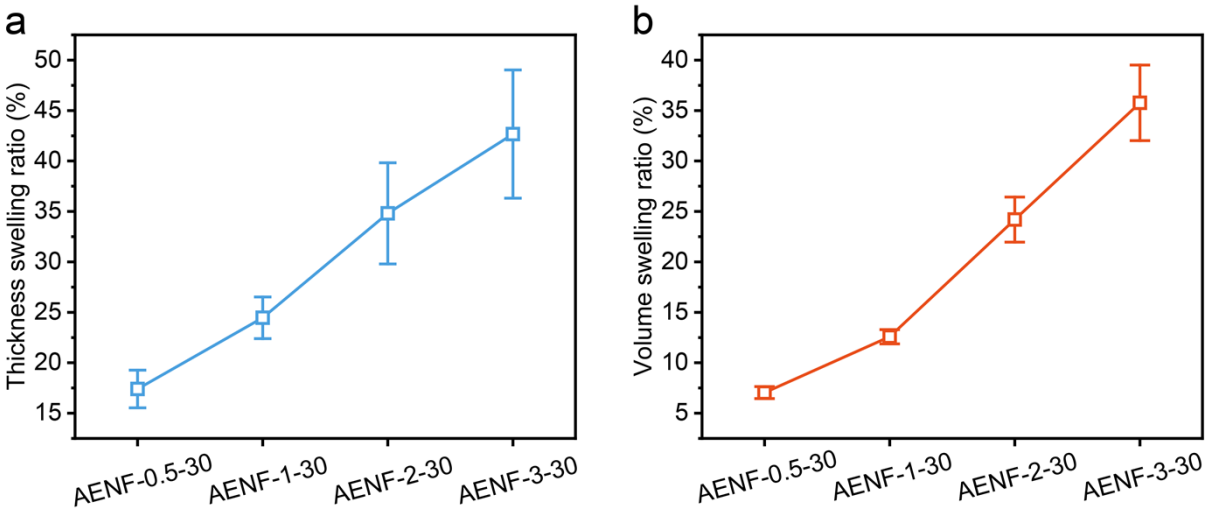

Figure S13. Swelling ratio of thickness (a) and volume (b) for AENF-*x*-30.

Figure S14. Bulk pH of the cathode electrolyte as a function of time for AENF-*x*-30.

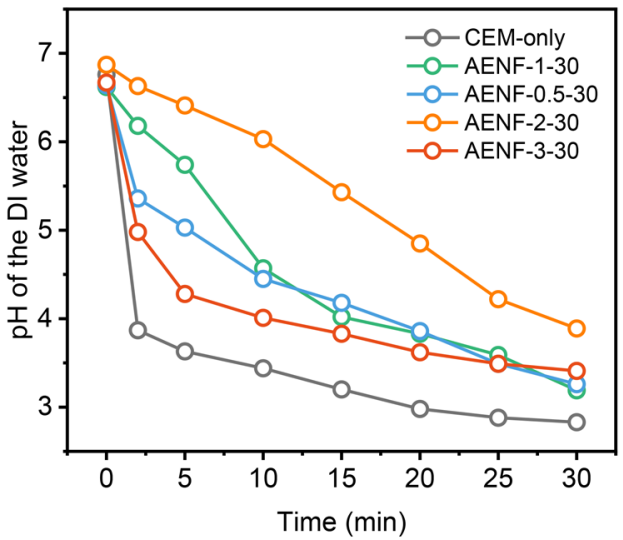

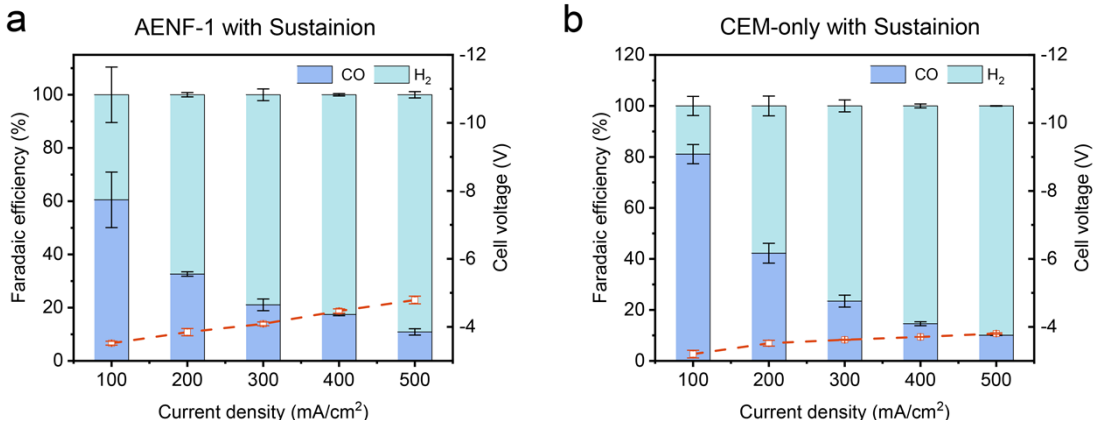

Figure S15. Faradaic efficiencies of CO (left axis) and the corresponding cell voltages (right axis) at varying current densities recorded from MEAs using (a) AENF-1 with Sustainion as

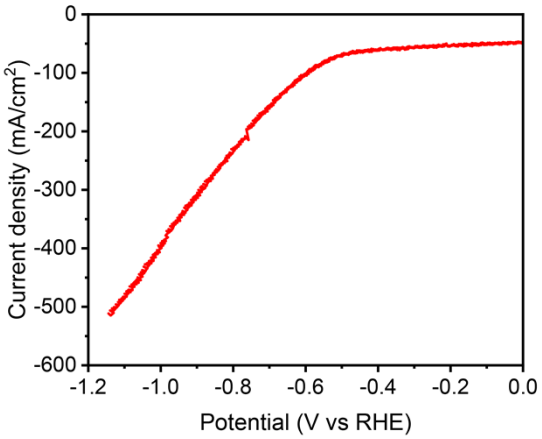

the cathode ionomer, (b) Nafion-HP with Sustainion as the cathode ionomer.

Figure S16. iR-corrected LSV curve of the three-compartment flow cell using 1 M $KHCO_3$, FAA-3-PK-130, and 1 M KOH as cathode electrolyte, AEM and anode electrolyte, respectively. Ni-N-C electrode, Ag/AgCl with saturated KCl, nickel foam was used as cathode, reference electrode and anode, respectively. The scan rate was10 mV/s.

Figure S17. iR-corrected LSV curve of a three-electrode system with IrO_2/Ti, graphitic rod, Ag/AgCl and 0.5 M H_2SO_4 as the working electrode, counter electrode, reference electrode and electrolyte, respectively. The scan rate was10 mV/s.

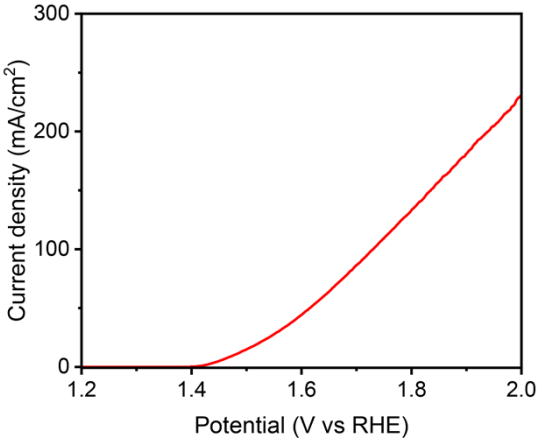

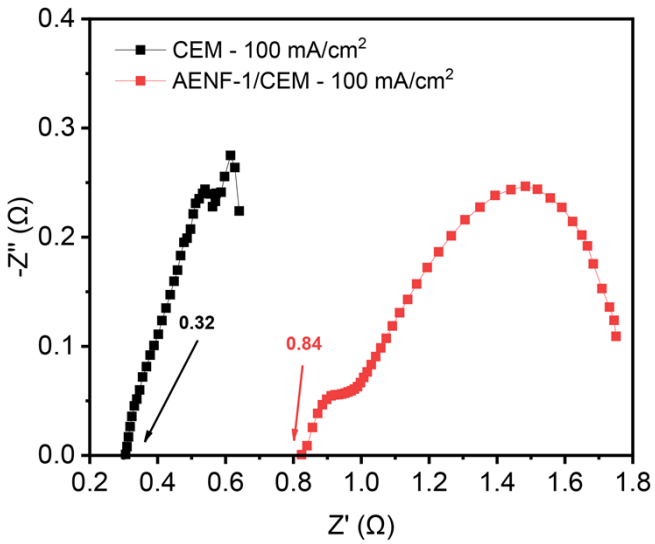

Figure S18. The Nyquist plot of MEA with CEM (black) or AENF-1/CEM (red), at the biased current density of 100 mA/cm^2. The 100 mA/cm^2 plot was recorded after stabilized for 15 min.

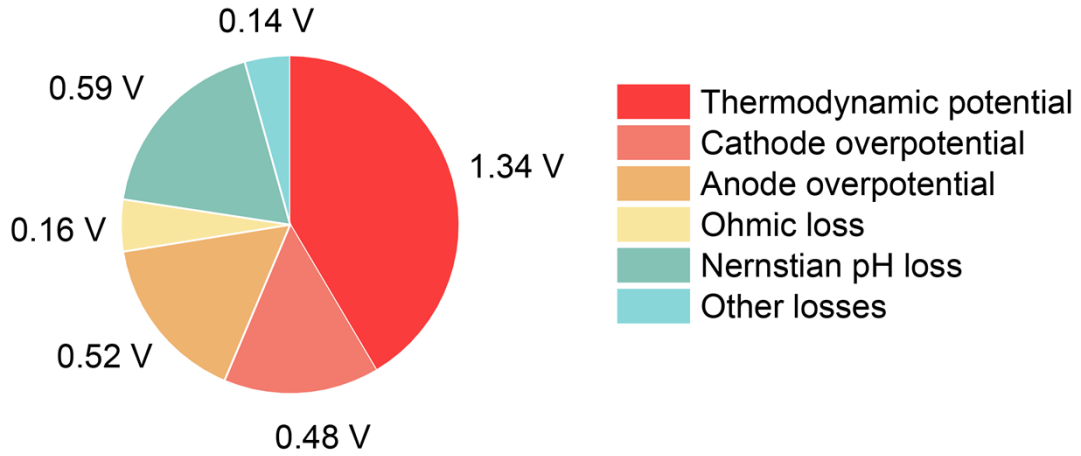

Figure S19. Cell voltage breakdown of the MEA with CEM-only.

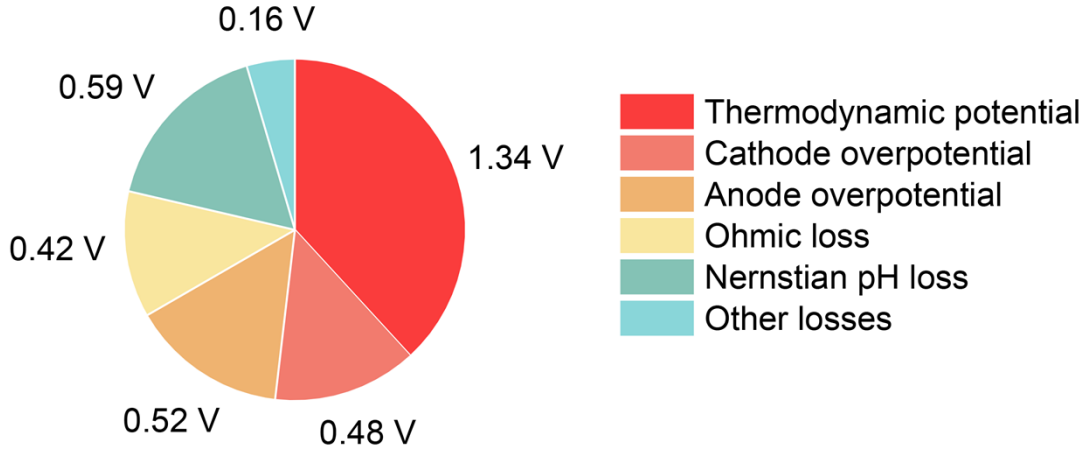

Figure S20. Cell voltage breakdown of the MEA with AENF-1.

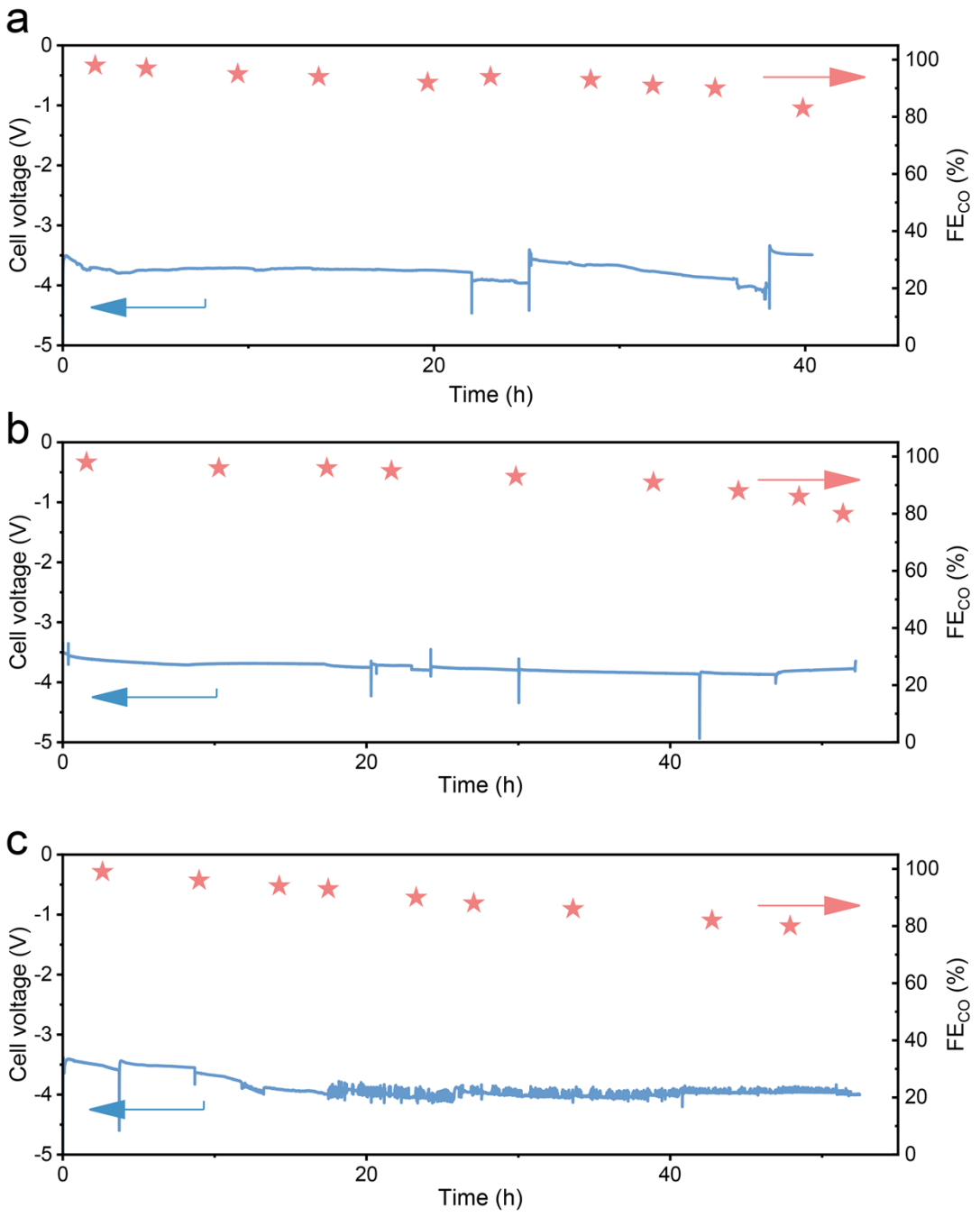

Figure S21. Galvanostatic eCO_2R tests of AENF-*x* in a 5-cm^2 acidic MEA at 100 mA/cm^2. (a) AENF-0.5, (b) AENF-2, (c) AENF-3.

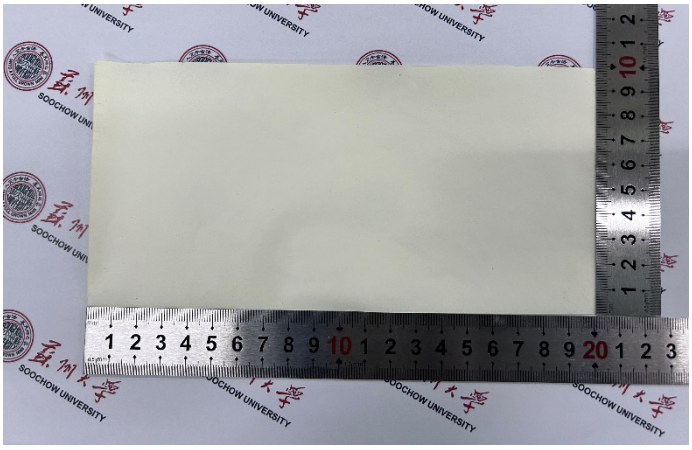

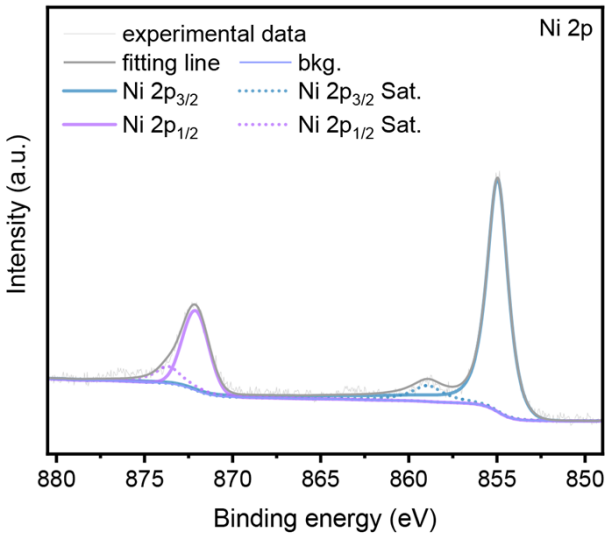

Figure S22. Optical image of a large-area electrospun membrane of AENF-1. (10 cm × 20 cm)

Figure S23. XPS Ni 2p spectrum of the pristine Ni-N-C catalyst before electrolysis.

Figure S24. XPS Ni 2p spectrum of the post-mortem Ni-N-C catalyst after prolonged electrolysis. Note the overlap of Auger F KL2 and XPS Ni 2p signals.

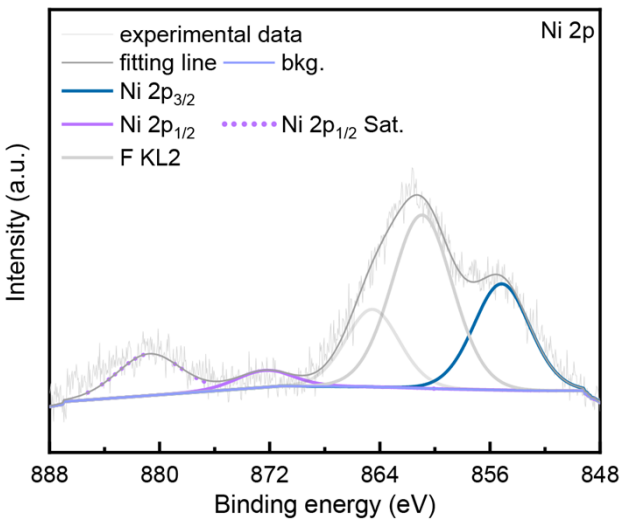

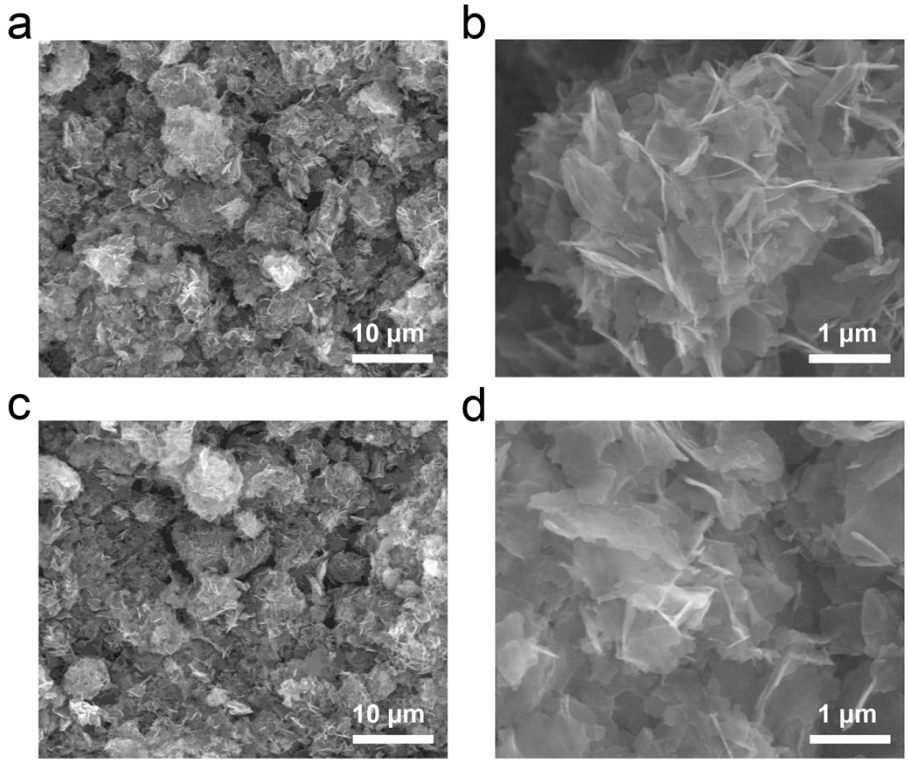

Figure S25. SEM images of the Ni-N-C catalyst (a, b) before and (c, d) after the stability test

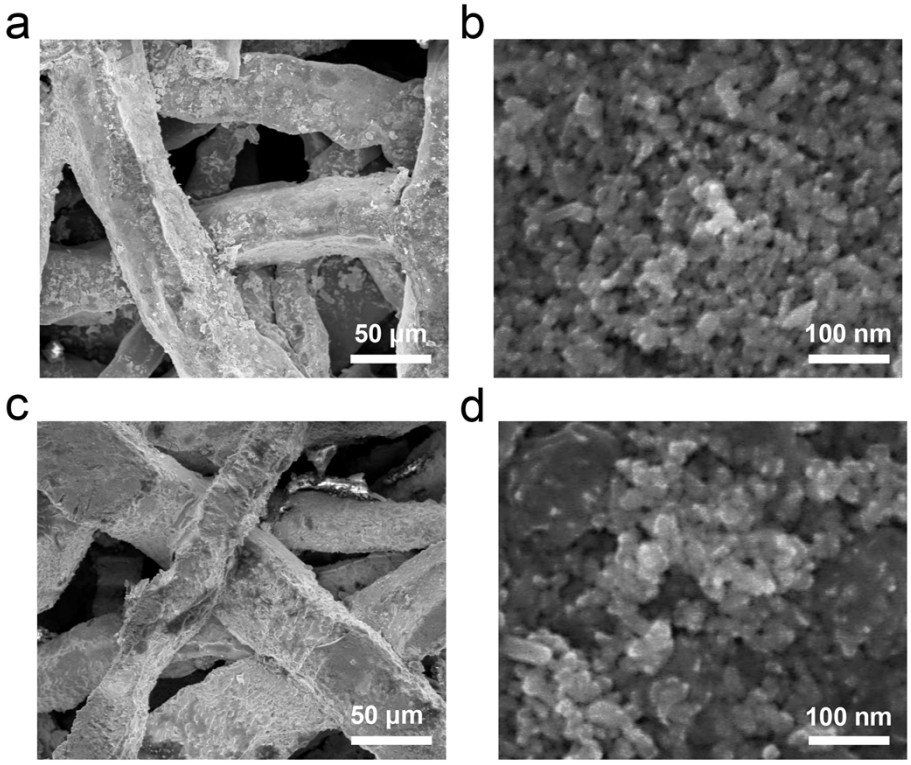

at 100 mA/cm^2 in acidic MEA with K_2SO_4/H_2SO_4 ($C_{K^+} = 0.05\ M$, pH = 2) as the anolyte.

Figure S26. SEM images of the IrO_2/Ti electrode (a, b) before and (c, d) after the prolonged

stability test at 100 mA/cm^2 in acidic MEA with K_2SO_4/H_2SO_4 ($C_{K^+} = 0.05\ M$, pH = 2) as the anolyte.

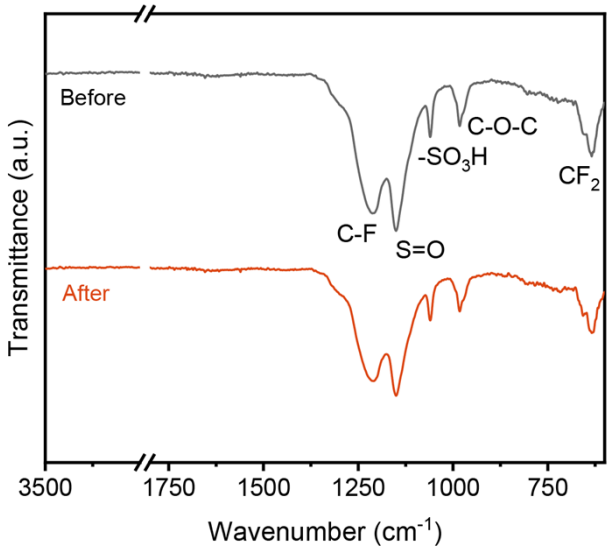

Figure S27. Infrared (IR) spectra taken on the Nafion-HP membrane before and after the prolonged stability test at 100 mA/cm^2 in acidic MEA with K_2SO_4/H_2SO_4 ($C_{K^+} = 0.05\ M$, pH = 2) as the anolyte.

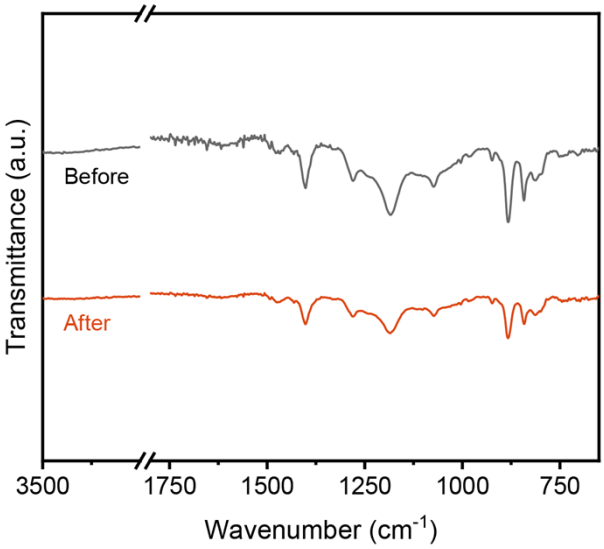

Figure S28. Infrared (IR) spectra taken on the AENF-1 membrane before and after the prolonged stability test at 100 mA/cm^2 in acidic MEA with K_2SO_4/H_2SO_4 ($C_{K^+} = 0.05\ M$, pH = 2) as the anolyte.

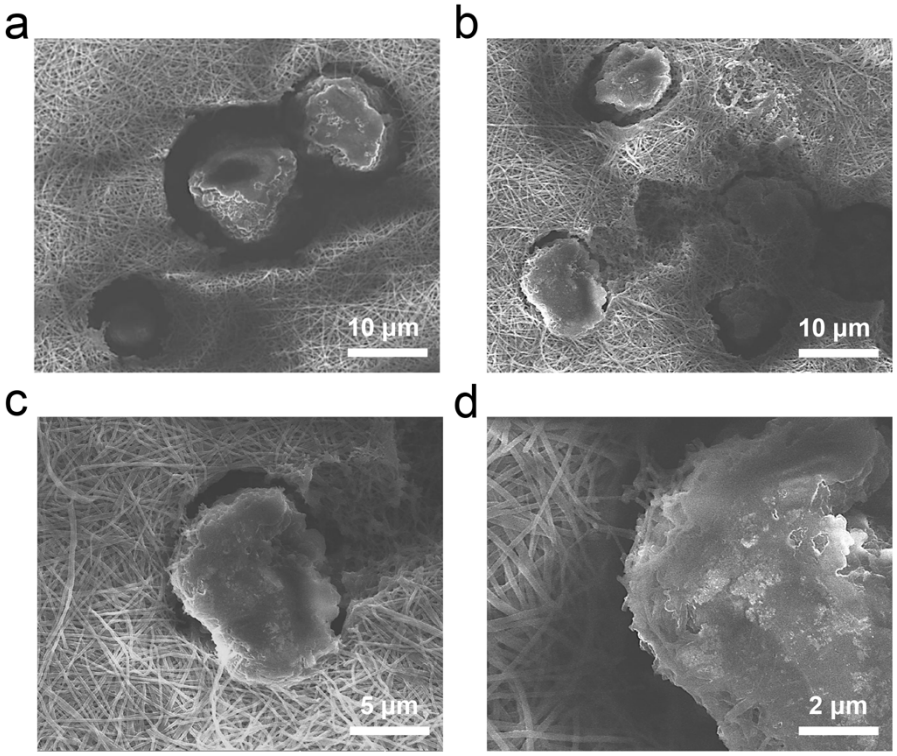

Figure S29. SEM images taken on the disassembled AENF-1 membrane after the prolonged stability test at 100 mA/cm^2 in acidic MEA with K_2SO_4/H_2SO_4 ($C_{K^+} = 0.05\ M$, pH = 2) as the anolyte.

Supplementary tables

Table S1. Summary of the average cell voltage, flooding rate and K^+ crossover rate estimated for AENF-*x*-*y*.

Samples	Average cell voltage	Flooding rate (mL/h)	K^+ crossover rate (mmol/h)
AENF-1-15	3.45 V	0.84	1.82
AENF-1-60	3.68 V	0.64	1.49
AENF-0.5-30	3.76 V	0.79	1.78
AENF-2-30	3.75 V	0.66	1.07
AENF-3-30	3.82 V	0.67	1.63
AENF-1-30	**3.51 V**	**0.709**	**1.37**

Table S2. Comparison of K^+ crossover rate in AENFs and AEM system.

System	Electrolyte	K^+ crossover rate (mmol/h)	Area (cm^2)	Ref.
AENF-1/Nafion HP	**pH = 2** **C_{K+} = 0.05 M**	**1.37**	**5**	**This Work**
AEM	0.05 M $KHCO_3$	0.1	5	[7]
AEM	0.1 M $KHCO_3$	0.135	6.25	[8]
AEM	0.1 M $KHCO_3$	0.015	1	[9]

Table S3. Properties of the flat-film of MTCP-50.

Property	Parameter
Thickness	35±3 μm
OH^- Conductivity	78.4 mS/cm
Water uptake	42%
Tensile strength	44.8 MPa
Swelling ratio	7.8%
Differential pressure	0.192 MPa

Table S4. Summary of the eCO_2R performances in acidic MEA reported in literature.

Catalysts	Membrane	j_{co}max (mA/cm^2)	Stability	Area (cm^2)	Electrolyte	Ref.
Ag/PTFE	CEM	105	50 h	5	pH = 1.84 C_{Cs+} = 0.02 M	[10]
Ni_5@NCN	CEM	222.8	15 h	5	pH = 0.6 C_{Na+} = 0.5 M	[11]
Ni-N-C	CEM	475	7.5 h	4	pH = 0.5 C_{K+} = 1 M	[12]
NiNF-1100	CEM	328	18 h	5	pH = 2 C_{K+} = 0.1 M	[13]
Au PTFE/ Ni–SAC	SSE/CEM	258	110 h	1	pH = 0.3	[2]
Ag/ PDDA-GO	CEM	210 110	50 h /	5	pH = 2 DI water	[14]
Ag	AEM/CEM (*f*-BPM)	256	200 h	4	DI water	[6]
Ag	AEI/CEM (*f*-BPM)	~380	200 h	1	DI water	[15]
Ni-N-C	**AENFs/CEM (*f*-BPM)**	**390**	**325 h**	**5**	**pH = 2** **C_{K+} = 0.05 M**	**This Work**
—	—	**281.6**	**110 h**	**25**	—	**This Work**

Table S5. Amount of Ni and Ir leaching in the cathode effusion and anolyte quantified by ICP-OES.

Condition	Ni leaching	Ir leaching
5cm^2-MEA stability test	under detection limit	under detection limit
25cm^2-MEA stability test	under detection limit	under detection limit

References

1. W. Song, K. Peng, W. Xu, X. Liu, H. Zhang, X. Liang, B. Ye, H. Zhang, Z. Yang, L. Wu, X. Ge and T. Xu, *Nat. Commun.*, 2023, **14**, 2732.
2. B. Wu, B. Wang, B. Cai, C. Wu, W. W. Tjiu, M. Zhang, Z. Aabdin, S. Xi and Y. Lum, *J. Am. Chem. Soc.*, 2024, **146**, 29801-29809.
3. K. Xie, R. K. Miao, A. Ozden, S. J. Liu, Z. Chen, C. T. Dinh, J. E. Huang, Q. C. Xu, C. M. Gabardo, G. Lee, J. P. Edwards, C. P. O'Brien, S. W. Boettcher, D. Sinton and E. H. Sargent, *Nat. Commun.*, 2022, **13**, 3609.
4. Y. Xie, P. Ou, X. Wang, Z. Xu, Y. Li, Z. Wang, J. Huang, J. Wicks, C. McCallum, N. Wang, Y. Wang, T. Chen, B. Lo, D. Sinton, J. Yu, Y. Wang and E. Sargent, *Nat. Catal.*, 2022, **5**, 564-570.
5. J. E. Huang, F. W. Li, A. Ozden, A. S. Rasouli, F. P. G. de Arquer, S. J. Liu, S. Z. Zhang, M. C. Luo, X. Wang, Y. W. Lum, Y. Xu, K. Bertens, R. K. Miao, C. T. Dinh, D. Sinton and E. H. Sargent, *Science*, 2021, **372**, 1074-1078.
6. J. Disch, S. Ingenhoven and S. Vierrath, *Adv. Energy Mater.*, 2023, **13**, 202400570.
7. S. Kato, S. Ito, S. Nakahata, R. Kurihara, T. Harada, S. Nakanishi and K. Kamiya, *ChemSusChem*, 2024, **17**, e202401013.
8. J. Biemolt, J. Singh, G. Prats Vergel, H. M. Pelzer and T. Burdyny, *ACS Energy Lett.*, 2025, **10**, 807-814.
9. S. Hao, A. Elgazzar, N. Ravi, T.-U. Wi, P. Zhu, Y. Feng, Y. Xia, F.-Y. Chen, X. Shan and H. Wang, *Nat. Energy*, 2025, **10**, 266-277.
10. B. Pan, J. Fan, J. Zhang, Y. Luo, C. Shen, C. Wang, Y. Wang and Y. Li, *ACS Energy Lett.*, 2022, **7**, 4224-4231.
11. Z. Liu, T. Yan, H. Shi, H. Pan, Y. Cheng and P. Kang, *ACS Appl. Mater. Interfaces*, 2022, **14**, 7900-7908.
12. H. Li, H. Li, P. Wei, Y. Wang, Y. Zang, D. Gao, G. Wang and X. Bao, *Energy Environ. Sci.*, 2023, **16**, 1502-1510.
13. M. Wang, L. Lin, Z. Y. Zheng, Z. Y. Jiao, W. Hua, G. W. Wang, X. X. Ke, Y. B. Lian, F. Lyu, J. Zhong, Z. Deng and Y. Peng, *Energy Environ. Sci.*, 2023, **16**, 4423-

4431.
14. J. Fan, B. Pan, J. Wu, C. Shao, Z. Wen, Y. Yan, Y. Wang and Y. Li, *Angew. Chem. Int. Ed*, 2024, **63**, e202317828.
15. M. Hesselmann, J. Lee, S. Chae, A. Tricker, R. Keller, M. Wessling, J. Su, D. Kushner, A. Weber and X. Peng, *ACS Appl. Mater. Interfaces*, 2024, **16**, 24649-24659.